

PARTICLE STRUCTURE ©

R. H. Dishington

April 2009

I. INTRODUCTION

For the last 100 years, particle physics has been successful primarily on the experimental side. The rare theoretical success has been the classification scheme called the "Standard Model", and the prediction of the existence of *one* particle. An extensive mathematical literature, e.g. string theory, N dimensions, etc., has done little to advance the knowledge of particle structure or predict particle masses.

The normal mutual support of theory and lab work has failed here, because QM is *non-visualizable* and suppresses *cause and effect*. This has guided experimentalists to the "bigger machine" approach; but particles are very flexible, and at some collision energy level they just come apart and new particles are formed. So, the limit has perhaps been reached in "bigger is better".

The job of laying out the whole field of particle structure will require a long effort by many investigators. The following is a small step in applying Main-Line physics to find a more flexible particle classification system and to point the way to a simpler, visualizable analytical picture.

II. PARTICLES

The ultimate goal is to change the present approach to particle structure by avoiding the difficulties of a dogged adherence to the use of successive layers of *point particles* to describe matter. Ascribing so many properties to point entities is at least unsatisfying. Of course, with only the rigor of the few presently known solutions of the field equations, the

following involves considerable *conjecture*. A good part of it could be wrong and later discarded. Nevertheless, the basic approach, i.e. extended particles rather than point particles, will surely continue to be part of any picture, for the simplicity and intuitive aspects are indispensable. The built in potential for specifying the masses of all the particles demands that attention be paid to this change in viewpoint. For the most part, processes empirically deduced from available measured data will be called upon for the visualization¹

Particles are distortions in the vacuum that can act as relatively concentrated units for some significant time. If the structure cannot change without some outside influence, the particle is stable. If it *must* redistribute itself into a new form (i.e. “convert”), it is unstable. In the simplest organization of particle categories, no distinction between stable and unstable particles is made; and stability is just another property. Based on the available information, there are only two different classes of fundamental particles:

1. Layered particles (layerons)
2. c particles (c-ons)

The c particles, photons and neutrinos, travel at the speed of light in free space, *and are quite different in structure from all the other particles*. Neutrinos allow conservation of spin angular momentum in particle interactions. Just how they carry electric energy away from interactions is not yet understood. Photons carry energy away from charged particles, generally orbiting. Some details of the c-on particles' makeup will be presented in a later Note.

1. Sources used here include: Phys.Rev.D, Particles and Fields, July (1996) Part I; D.H.Perkins, Introduction to High Energy Physics, 2nd Ed. Addison-Wesley Publ.Co. Mass. (1982); B.C.Duff, Fundamental Particles, Taylor & Francis, London & Philadelphia (1986); F.Halzen & A.D.Martin, Quarks and Leptons, John Wiley & Sons, N.Y. (1984); I.S.Hughes, Elementary Particles, 2nd Ed. Cambridge U. Press(1985); R.N.Cohn&G.Goldhaber, The Experimental Foundations of Particle Physics, Cambridge U. Press (1989).

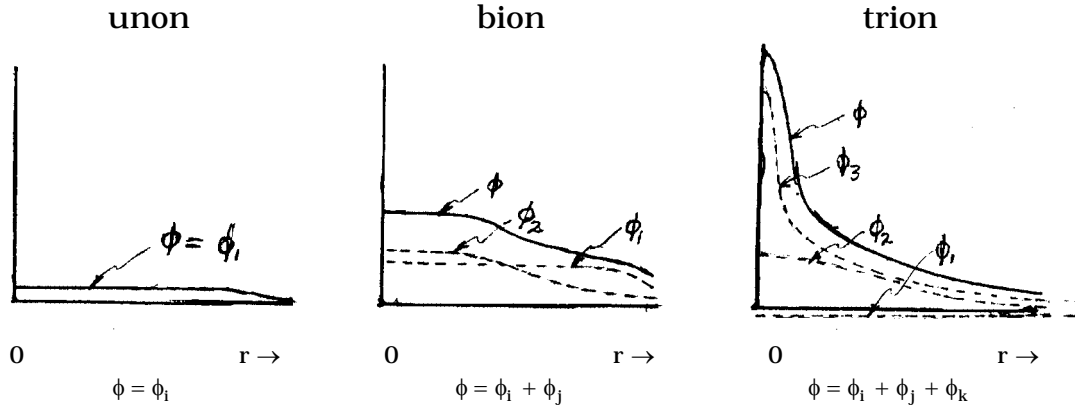


Figure 1. Layered particles.

The layered particles are composed of spherically symmetrical distortion components, in some ways similar to the electron, supported by ℓ -waves and stacked in various arrangements of potential ϕ (see Figure 1). Examples of 1, 2, and 3 layered particles are the positron, pion, and proton respectively. In the following, the layerons will be discussed in detail. The separation of layerons and c-ons helps to emphasize that layerons are bulk distortions with purely *electric* energy. A proper analysis of the layerons begins with the unons, for which the theory is much advanced. The subsequent description of the bions and trions is far from complete, and leans heavily on the unon analysis. Nevertheless, the *visualization* is carried to the point where, even without the final rigorous answers to many important questions, the overall picture is almost totally understandable and only awaits the formal filling out of the many specific cases.

III. PARTICLE MEASUREMENTS

Many of the particle types studied by physicists are man-made, and only a very few are involved in the structure of the world (e, p, n). TABLE I lists the most important particles and shows their decay products, which help to visualize how the particles are constructed.

Numerous other vacuum disturbances, called *resonances*, have some particle-like behavior, but here they are not considered to be particles.

In spite of the fact that most of the data used to describe particle characteristics at present are obtained by high energy collisions of beams and targets, and that this information is indispensable, it is not of paramount importance here where the goals are somewhat different.

TABLE I

PARTICLE CONVERSION PRODUCTS

	<u>Products</u>	<u>Percent</u>
<u>Unons</u>		
$e^\pm \rightarrow$	stable	
$\mu^- \rightarrow$	$e^- \bar{\nu}_e \nu_\mu$	100
$\tau^- \rightarrow$	$\mu^- \bar{\nu}_\mu \nu_\tau$	18
	$e^- \bar{\nu}_e \nu_\tau$	17
	bions, c-ons	65
<u>Bions</u>		
π^0	$\gamma\gamma$	98.8
	$\gamma e^+ e^-$	1.2
π^-	$\mu^- \bar{\nu}_\mu$	100
η	$\gamma\gamma$	39.3
	$3\pi^0$	32.1
	$\pi^+ \pi^- \pi^0$	23.2
	$\pi^+ \pi^- \gamma$	4.8
	K^+	$\mu^+ \nu_\mu$
K^+	$\pi^+ \pi^0$	21.2
	bions, unons	15.3
All others yield mixes of bions, trions and c-ons		
<u>Trions</u>		
$p \rightarrow$	stable	
$n \rightarrow$	$pe^- \bar{\nu}_e$	100
$\Lambda^0 \rightarrow$	$p\pi^-$	63.9
	$n\pi^0$	35.8
$\Sigma^+ \rightarrow$	$p\pi^0$	51.6
	$n\pi^+$	48.3
$\Sigma^0 \rightarrow$	$\Lambda\gamma$	100
$\Sigma^- \rightarrow$	$n\pi^-$	100
All others yield mixes of bions, trions and c-ons		

Instead, the discussion will lean toward particle decay, because only the electron and the proton (and the neutron when part of a nucleus) are stable. All other particles decay in a relatively short time after formation. The only difference between the bombardment and decay conversion processes is in the complexity of the initial conditions. Particle conversion involves only *one* pseudo-stable or unstable particle that redistributes its distortion to a lower energy configuration.

In particle *decay*, energy distortion, uninfluenced by any outside presence other than the datum fluctuation, will always redistribute in a downhill direction, i.e. produce only constituents of energies smaller than the original (all adding up to the original energy, of course). This means that any of the particles to be examined will convert to one or more of those listed in Table I at lower energies only. These are not the only conversions the listed particles undergo, but those omitted, which may be very numerous in type, are found only a small fraction of the time, less than a few percent, and often as little as, say, 10^{-6} percent.

IV. UNONS

The most common single layer particle is the electron/positron, which was discussed in detail in Notes 1 and 2. Referring back to those Notes, the e/p is a single dip (bump) of electric potential ϕ (hlu),

$$\phi = \phi_0(1 - \psi^2) \quad , \quad (1)$$

where $\psi = \varepsilon^{-r_i/r}$ is the intrinsic ℓ - wave shape function. This single layer of potential yields single layers of energy and charge density, which indicates that the e/p is a unon with total rest energy and charge (hlu),

$$E_0 = 2\pi\phi_0^2 r_i \quad \text{and} \quad q = 8\pi\phi_0 r_i \quad . \quad (2)$$

It is important to recognize that the solution of Eq.(7), in Note 1, for the ℓ -wave shape function was in no way specific to the electron. Only when the particular inflection radius $r_i = 3.522 \times 10^{-14}$ cm was used there in Eq.(8) [or (1) above] did the rest energy E_0 , of the bulk distribution ϕ , identify the particle as the electron.

Actually, a shortcut was used to find r_i in Note 1, where the known values of the electron's E_0 and charge e^\pm were used to calculate it. However, as described in Note 3, the fundamental and proper way to find r_i and ϕ_0 is to begin with the *measurement* of the unon's ℓ -wave frequency ν through its connection to the Rydberg constant. The latter procedure can be extended to the other unons. In an important series of experiments done between 1954 and 1957¹ by Stearns, et al, various materials were bombarded with μ^- or π^- particles, and the spectra of the μ^- or π^- atoms, in which an electron was replaced by the μ^- or π^- , were measured. By a Rydberg calculation similar to the one for the electron, ν_μ was found to be very close to the value used in the present work. Once the ℓ -wave frequency is known, the derived relationship [Note 3, Eq.(14)],

$$E_0 = h\nu \quad , \quad (3)$$

provides the unon's rest energy, and its other characteristics can be worked out.

Because the basic measurement of ℓ -wave frequency just described is difficult, particularly for higher energy unons with very short lifetimes, the more practical shortcut is used in this Note and ν_μ and ν_τ are again calculated from their *measured* bulk rest energies.

1. M.B.Stearns, in Progress in Nuclear Physics, **6**, 108-137 (1957); M.B.Stearns & M.Stearns, Phys. Rev., **105**, 1573-82 (1957).

The Energy Compaction Relationship

Eliminating ϕ_0 between the rest energy E_0 and charge q found in Eqs.(2) above (hlu),

$$E_0 r_i = \frac{q^2}{32\pi} \quad \text{erg - cm} \quad , \quad (4)$$

a relationship called the *energy compaction equation*. It indicates that the more energetic unons have smaller radii. For $q = e^\mp$, $E_0 r_i = 2.8838 \times 10^{-20}$ erg-cm .

Unon Size and Stability

The unons of interest will be limited to the series of whole charged particles, i.e. e, μ, τ, \dots , that can exist alone and be observed for some finite time. Using the compaction relationship derived above, and the measured values of E_0 for each of the unons, the calculated values for r_i and ϕ_0 are listed in TABLE II with each particle's observed mean life.

TABLE II
UNONS, THE "PREFERRED" VACUUM STATES

E ₀ (ergs)	r _i (cm)	φ ₀ (hvolts)	mean life (s)
e 8.1871 × 10 ⁻⁷	r ₁ = 3.5224 × 10 ⁻¹⁴	1.9233 × 10 ³	Stable
μ 1.6929 × 10 ⁻⁴	r ₂ = 1.7035 × 10 ⁻¹⁶	3.9768 × 10 ⁵	2.1970 × 10 ⁻⁶
τ 2.8472 × 10 ⁻³	r ₃ = 1.0129 × 10 ⁻¹⁷	6.6886 × 10 ⁶	2.9100 × 10 ⁻¹³

The interesting features of TABLE II are that, first, although each of these unons has the same charge e^\mp the more energetic particles have larger center potentials; and, their energy being packed into a smaller volume correlates with their being less stable. Second, it appears that the unon sequence is a set of *preferred* vacuum states that can exist as "pseudo-stable" particles *because of some fundamental property of the vacuum*. TABLE III lists the important "rest" characteristics of the three known unons.

TABLE III

UNONS

Electron e	Muon μ	Tau τ
$\tau_e = \text{Stable}$	$\tau_\mu = 2.1970 \times 10^{-6} \text{ s}$	$\tau_\tau = 2.910 \times 10^{-13}$
$E_{0e} = 0.51100 \text{ MeV}$	$E_{0\mu} = 105.66 \text{ MeV}$	$E_{0\tau} = 1,777.1 \text{ MeV}$
$r_e = 3.5224 \times 10^{-14} \text{ cm}$	$r_\mu = 1.7036 \times 10^{-16}$	$r_\tau = 1.0129 \times 10^{-17}$
$q_e = 1.7027 \times 10^{-9} \text{ hIc}$	$q_\mu = q_e = e$	$q_\tau = q_e = e$
$\phi_{0e} = 1923.3 \text{ hIV}$	$\phi_{0\mu} = 3.9768 \times 10^5$	$\phi_{0\tau} = 6.6886 \times 10^6$
$\sigma = \frac{h}{4\pi} = 5.2729 \times 10^{-28} \text{ erg-s for all } \rightarrow$		
$\mu_e = 3.2910 \times 10^{-20} \frac{\text{erg}}{\text{hIG}}$	$\mu_\mu = 1.5920 \times 10^{-22}$	$\mu_\tau = 9.4258 \times 10^{-24}$
$m_e = 9.1094 \times 10^{-28} \text{ g}$	$m_\mu = 1.8835 \times 10^{-25}$	$m_\tau = 3.1679 \times 10^{-24}$
$\omega_e = 7.7634 \times 10^{20} \frac{\text{rad}}{\text{sec}}$	$\omega_\mu = 1.6052 \times 10^{23}$	$\omega_\tau = 2.6998 \times 10^{24}$

V. PREFERRED VACUUM STATES

The μ and τ are often called "big electrons", because, like the electron, they have only the same two simple characteristics, their center potentials and their inflection radii. In the later discussion of multi-layer particles, it becomes clear that the multiple layers are similar to these three unons. In fact, *the radii of the layers in multi-layer particles are essentially the same as those listed in TABLES II AND III*. In one way this

is surprising, but why it is true can be understood better from the following.

The Layer Radius/Frequency Equation

An important relationship between the inflection sphere radius of a unon and the unon's ℓ – wave frequency is obtained by eliminating E_0 from Eqs.(3) and (4), with the result,

$$\omega_i r_i = \frac{q^2}{16h} = D \quad , \quad (5)$$

where $D = e^2/16h = 2.7346139 \times 10^7$ rad-cm/s. Figure 2 depicts this relationship for the unon family of particles. Eq.(5) takes the surprise out of the concept of preferred vacuum states, for although it is difficult to imagine how preferred *radii* could be a basic condition in the vacuum, it is comfortable to think of preferred vacuum *frequencies* as basic. So, assuming that Figure 2 indicates that the vacuum has preferred *frequency* states, Eq.(5) shows that this also establishes preferred radii.

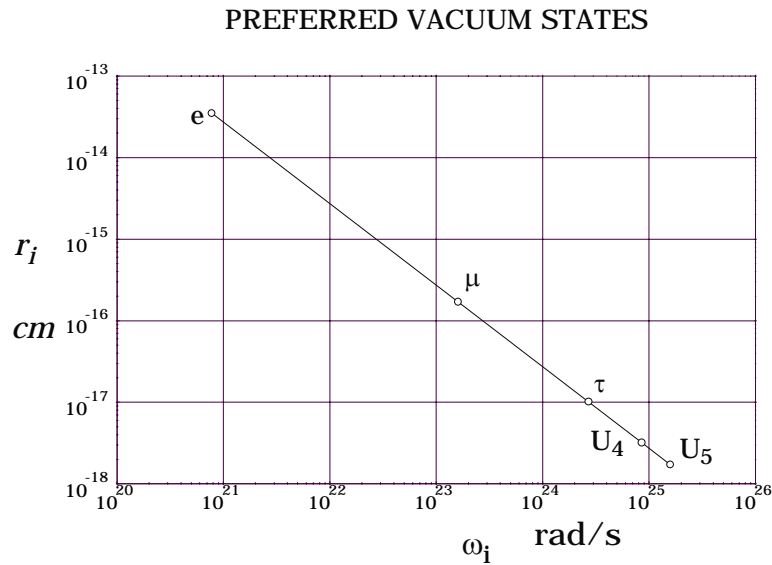


Figure 2

Figure 2 indicates two possible unons, U_4 and U_5 , *that have not yet been observed*. Later on, in analyzing the more massive, composite particles, it is apparent that there are at least two more preferred states,

4 and 5; but their great compactness and instability may make their existence possible only inside the composite particles and not observable as unons of higher order. The values shown are *educated guesses*.

Quarks

From the 1960's on, it has been understood that the more elaborate particles are constructed of objects, now called quarks, that sometimes behave in a manner similar to unons but have fractional charges $\pm e/3$ and $\pm 2e/3$. They are thought to be "point" charges like the conventional electron model. *Little is known about the spatial arrangement of these objects inside a composite particle.*

In interactions between quarks and external projectile particles, the *quarks behave as if they were independent entities, but no individual quark has ever been observed outside its housing particle.* This suggests that the composite particles might be made up of very flexible constructs similar to the finite unons described earlier, but having fractional charges, two components for the mesons and three for the baryons. In that case, although the components might freely move for short distances, if one of the components were forced out of a composite particle, because of its fractional charge, it would not qualify as one of the preferred unon solutions listed in TABLE II, and so would decay; as would the remaining debris from the original particle. If this is a correct description of composite particles, then all of the properties of the Standard Model are preserved and yet a greater flexibility results.

The classification scheme described in the following includes all *whole* charge particles, but not photons and neutrinos. Using the Standard Model as a guide, the two "point" quarks that make up mesons and the three "point" quarks that make up baryons are replaced with the finite solutions of Eq.(1). To avoid confusing the properties of the "point" quarks with these finite constructs, the term quark will not be used to describe the particle components.

VI. PARTICLE CLASSIFICATION

Whereas the quarks have specific charges assigned, the present scheme first indicates only the number of components a particle has. The basis for the nomenclature system is represented in Figure 3. The numbered markers represent the relative radii of layers, *which are **not** equally spaced*, indicating only the stacking order. The unons, bions and trions are designated by U_i , B_{ij} ($i \leq j$) and T_{ijk} ($i < j < k$) respectively, *where the i, j and k indicate the layers, and read from the outermost layer inwards.* The possibility that “quadrons” also exist can be accommodated by writing Q_{ijkl} , etc. In all these cases, *the Eq.(1) constructs take on only the preferred radii listed in TABLE II*, so the subscripts indicate the size and shape of the components.

In this system, the correspondence of the U_i designation to the unon family listed in TABLE II is, $U_1 \rightarrow e$, $U_2 \rightarrow \mu$ and $U_3 \rightarrow \tau$, etc., each successive particle having a single potential structure with a higher frequency, a smaller radius and a greater energy (see Figure 1). The total charge of each is $\pm e$.

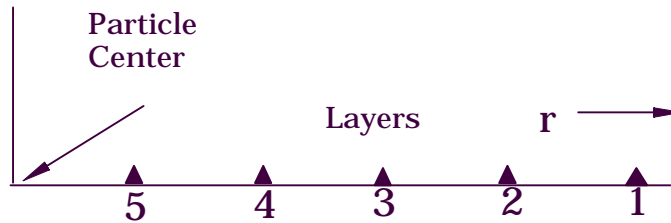


Figure 3. The preferred layer radii order.

When considering the multi-layer particles, several new characteristics appear. For example, *the individual layers do **not** have different frequencies, each multi-layer particle has just one basic frequency ω , and a single ℓ -wave establishes all the layers.* The frequency ω will

not be one of the "preferred" layer frequencies. Instead, the single ℓ – wave of a multi-layer particle acts like a driver that *rings* the two or three "preferred" layers constituting that particular particle. For example, the proton will be shown to have the structure T_{123} ; i.e. a potential component ϕ_1 with inflection radius r_1 , a higher potential component ϕ_2 with smaller inflection radius r_2 , and a very high potential component ϕ_3 with a still smaller inflection radius r_3 (see Figure 1). On the other hand, there could be another trion T_{245} , with components ϕ_2 , ϕ_4 and ϕ_5 , and inflection radii r_2 , r_4 and r_5 . Only those "preferred" radii given in TABLE II and the possible r_4 and r_5 , still to be determined accurately, ever appear in the *components* of multi-layer particles; but, each multi-layer particle has just one ℓ – wave frequency ω .

It is convenient to set up the next step in the classification system on the basis of the smoothed out charge density shell ρ rather than the potential ϕ or the energy density shell ε_e , since the total integrated charge of any shell is constant, even when the particle is in motion. The conventional "Standard Model" adopts a very rigid classification scheme that *combines* the layers and charges in a way that is too inflexible. The increased flexibility of the new system comes from the fact that the *charges* of each component have yet to be specified. Now it appears that *all independent, observable particles have total charges that are integral multiples of e*. Because of this empirically determined fact the *total* particle charge distortion is $\pm Ne$, where N is an integer; so, at least in the two layer particles with charge e, *some of the layers must have fractional charge*. The fractional charges have been found to be either $\pm e/3$ or $\pm 2e/3$.

In the present system, *the charge sign and magnitude are indicated, separately from the layers, by superscripts*. For example, the proton is

identified as the trion T_{123}^{-++} where the superscripts indicate that the fractional charges of the components are $-e/3$, $+2e/3$, $+2e/3$. The neutron is tentatively identified as T_{123}^{-+-} . Thus, $B_{ij}^{\alpha\beta}$ ($i \leq j$) and $T_{ijk}^{\alpha\beta\gamma}$ ($i < j < k$) represent the complete description of the multi-layer particle categories (except for the spins), where α, β, γ are given values of $\overset{+}{1}$, $\overset{-}{1}$, $\overset{+}{2}$, $\overset{-}{2}$, $\overset{+}{3}$, or $\overset{-}{3}$ for the six possible charge choices. Here, $\overset{+}{1}$ indicates a charge of $+e/3$, $\overset{-}{2}$ a charge of $-2e/3$ and $\overset{+}{3}$ a charge of $+e$.

Bion Configurations

Bions are classified into three groups:

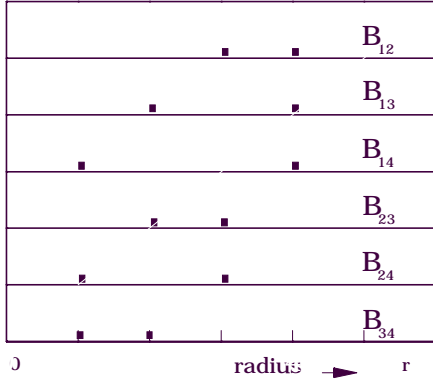
- | | | | |
|--------------------------------------|---|----------|---------|
| 1. Concentric layer bions, | } | B_{ij} | $i < j$ |
| 2. Eccentric layer, inside orbiters, | | | |
| 3. Outside orbiters | | B_{ii} | |

Group 1 bions have two shells, one inside the other, with a common center. They have a net charge of e^\pm , whereas the orbiters have two layers of equal and opposite charge that give a net charge of zero. Group 2 bions have two shells, one inside the other, with centers displaced and both orbiting a common center. Group 3 bions form a "system" like positronium, with two separated, equal fractional charge shells, orbiting a common center. Observed *concentric* bions are tentatively identified as π^\pm , D^\pm , D_s^\pm , and B^\pm . *Inside orbiter* bions are probably K^0, D^0, B^0 and B_s^0 and *outside orbiter* bions are most likely $\pi^0, \eta, \eta', \eta_c$ and Υ . The latter decay like Positronium and, similarly, produce two photons. *This two photon radiation is their hallmark.*

All the bions are possibly stable, in a fundamental sense (if it were not for the datum fluctuations), but *all bions convert to lower energy forms*

shortly after their formation. Because the bions decay rapidly, their correct analysis must address the transient case, which has many mathematical difficulties. Therefore, the measured bion energies are always slightly smaller than the values calculated from the "concentric, static" approximation.

Figure 4 diagrams the first six forms of the B_{ij} bion hierarchy. For



The B_{ij} bion hierarchy
Figure 4.

each of these B_{ij} designations, there are *several* possible charge combinations. For complete generality the charges 3^+ and 3^- were included earlier; but in the following, to relate to the present view of quarks, the 3^+ and 3^- categories will not be developed for bions. As an example, consider the lowest order bion category $B_{12}^{\alpha\beta}$. Each of the

two layers could have one of four different charge distortions, so the total possible types of B_{12} bions is 16. However, this number is reduced considerably because the total particle charge must be zero or an integral multiple of $\pm e$. Therefore, the total number of combinations that could possibly represent real particles is reduced to:

$$B_{12}^{+-}, B_{12}^{++}, B_{12}^{+-}, B_{12}^{--},$$

and,

$$B_{12}^{-+}, B_{12}^{--}, B_{12}^{+-}, B_{12}^{++}.$$

Now, since the second row represents four particles that are exactly like those in the first row, except that their charges are opposite, the second row particles are called the "anti-particles" of those in the first row. Thus, the B_{12} category describes only four different, possible particles (and

their anti-particles). Subsequent analysis can help to decide which, if any, is a real particle and to identify one or all with those observed. The charge density distributions of the tentative B_{12}^{++} particle and its anti-particle are depicted in Figure 5. A similar process can be carried out for all B_{ij} bions. The result is that each bion category can have only four possible particles (and their anti-particles):

$$B_{ij}^{+-}, B_{ij}^{++}, B_{ij}^{+-}, B_{ij}^{--} . \quad (6)$$

The first and last of these are inside orbiters, the second and third are concentric bions.

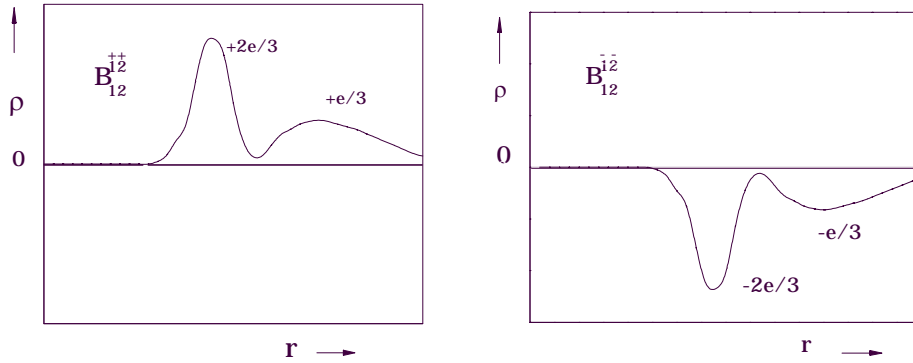


Figure 5. Examples of possible B_{12} bions.

Unlike the unon family, which has a “stable” particle, the electron, at the base of its energy ladder, the bions are all short lived, and even the lowest energy B_{ij} bion is triggered to convert into unons and neutrinos. No more need be said about B_{ij} bions until later.

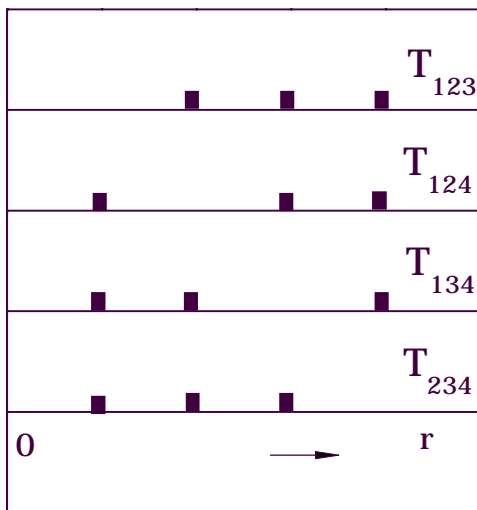
In the most general case of the outside orbiter category, each $B_{ii}^{\alpha\beta}$ yields only three possible types of bions (they are their own anti-particles):

$$B_{ii}^{+-}, B_{ii}^{+-}, B_{ii}^{+-} . \quad (7)$$

The last, B_{ii}^{33+-} , is essentially positronium, which is not considered a *fundamental* particle. Analysis of all orbiters involves more than just solving the ℓ -wave equation, which only gives the structure of the layers themselves. Because orbiters are “systems” over and above the layers, they require an analysis that shares the orbit matching properties of atomic systems.

Trion Configurations

The trions come in combinations of *concentric* shells, or *eccentric inside orbiters*. Although work is in progress, the only accurately calculable concentric trion at this time is the stable proton. The great majority of trions appear to be *inside* orbiters, none of which has been finally identified yet due to mathematical intractability. The success of the proton analysis demands that the much more difficult problem of the



orbiter trions be pursued, particularly that of the neutron.

The same procedure that established the possible bions is applicable to the trions as well. However, in the basic trion hierarchy, there might not be outside orbiters. Thus, for now, the *basic* trion configurations given here involve only concentric cases of $T_{ijk}^{\alpha\beta\gamma}$ where

$i < j < k$. The result is that the first few T_{ijk}

appear as in Figure 6. Each of these

The concentric trion hierarchy.
Figure 6.

categories has 3 layers, and each layer can have one of 4 possible charges, so every category has 64 *possible* particles. Here, again, the requirement for $\pm Ne$ ($N=0,1,2,\dots$) total particle charge reduces the number of possibles to one out of eight, or 8 (plus their anti-particles). Subsequent analysis can reduce this number.

The *proton* is the only “stable” trion known. Again, all concentric trions might be *basically* stable but open to triggering into conversions by the datum fluctuations, which accounts for their short lifetimes. The proton, however, is stable, the lowest sustainable trion form, just as the electron, at the bottom of the unon energy ladder, is stable.

The charge assignments for the 8 tentative trions of each set are:

$$\begin{array}{cccc} \bar{1}\bar{1}\bar{1} & \bar{1}\bar{1}\bar{2}^+ & \bar{1}\bar{2}\bar{1} & \bar{1}\bar{2}\bar{2}^+ \\ \bar{2}\bar{1}\bar{1} & \bar{2}\bar{1}\bar{2}^+ & \bar{2}\bar{2}\bar{1} & \bar{2}\bar{2}\bar{2}^+ \end{array}$$

Each of the T_{ijk} categories can have these charge assignments and their negatives. The advantage of this classification system over the standard model is that it frees the charge assignments from the quarks and provides the layer visualization, which is simple to use and to remember.

VII. MULTI-LAYER PARTICLE ANALYSIS

Analysis of *concentric* multi-layer particles runs parallel to the unon derivation of Notes 1 and 2, and Section IV of this Note. Figure 7 lists the principal steps involved.

UNON ANALYSIS

1. Assume a simple trial potential.

$$\phi = \phi_0(1 - \psi_i^2)$$
2. Find a correct ℓ - wave shape function.

$$\psi_i = \varepsilon^{-r_i/r}$$
3. Solve for the correct charge density.

$$\rho = -\nabla^2\phi = 4 \frac{\phi_0 r_i^2}{r^4} \varepsilon^{-2r_i/r}$$

Figure 7. Unon analysis outline

Although the multi-layer equations are more elaborate, the outline in Figure 8 shows that roughly the same steps are necessary to determine the layered particle's characteristics.

MULTI-LAYER ANALYSIS

1. Assume a trial potential.

$$\phi = \phi_0(1 - \psi^2) = \phi_{01}(1 - \psi_1^2) + \phi_{02}(1 - \psi_2^2) + \phi_{03}(1 - \psi_3^2) + \dots$$
2. Find each layer's generalized ℓ - wave shape function.

$$\psi_i = \epsilon^{-\frac{r_e}{r}} \left[1 + K_i E_2\left(\frac{r}{r_e}\right) \right]$$

(r_e is the *effective* radius of the whole particle)
3. Find the K_i for each layer.

$$K_i = \left(\frac{r_i}{r_e} - 1 \right) \epsilon^{r_i/r_e} = \left(\frac{\omega}{\omega_i} - 1 \right) \epsilon^{\omega/\omega_i}$$
4. Solve for the correct layer charge densities.

$$\rho_i = -\nabla^2 \phi_i = \frac{q_i r_e}{2\pi} \left(1 + K_i \epsilon^{-r/r_e} \right) \frac{\psi_i^2}{r^4}$$

Figure 8. Multi-layer analysis outline

In the following, the steps in Figure 8 are elaborated upon and the method is applied to *concentric* bions and trions.

Earlier it was said that *all* unons had charge distortion $\pm e$. When multi-layer particles are observed, at least two types are found to have a total charge of $\pm 2e$. To simplify the presentation, the examples that follow apply only to particles with total charge $\pm e$. Certain small changes are required to deal with the $\pm 2e$ particles.

A Trial Potential

Although later the proton will be used as an example, it is straightforward to generalize the process for any *concentric* particle. The principal idea is that, as discussed in Note 1 under the energy density correction, the only *physical presence in a particle layer is its potential* ϕ_i ; so, in the multi-layer particle, *the only physical presence is the **sum** of the potentials* ϕ_i of the particle's layers (see Figure 1),

$$\phi = \phi_1 + \phi_2 + \phi_3 + \dots \quad , \quad (8)$$

Paralleling the unon derivation, the same simple form of trial solution of Maxwell's scalar equation is taken as,

$$\phi = \phi_0(1 - \psi^2) \quad , \quad (9)$$

where ψ is the multi-layer shape function. In terms of the individual layer potentials, this becomes,

$$\phi = \phi_{01}(1 - \psi_1^2) + \phi_{02}(1 - \psi_2^2) + \phi_{03}(1 - \psi_3^2) + \dots \quad , \quad (10)$$

which reduces to,

$$\phi = \phi_0 - (\phi_{01}\psi_1^2 + \phi_{02}\psi_2^2 + \dots) \quad , \quad (11)$$

where,

$$\phi_0 = \phi_{01} + \phi_{02} + \phi_{03} + \dots \quad . \quad (12)$$

The ϕ_{0i} 's can each be positive or negative.

The Multi-layer Shape Function

Comparing Eqs.(9) and (11),

$$\psi^2 = \frac{\phi_{01}}{\phi_0}\psi_1^2 + \frac{\phi_{02}}{\phi_0}\psi_2^2 + \frac{\phi_{03}}{\phi_0}\psi_3^2 + \dots \quad , \quad (13)$$

where the ϕ_{0i}/ϕ_0 are fractions related to the amount of charge in each layer of the composite particle. Eq.(13) defines the *total* multi-layer shape function ψ ; and, because the ψ_i of the layers are not equal, the total shape function has more wiggles than the unon shape function, as shown in Figure 9.

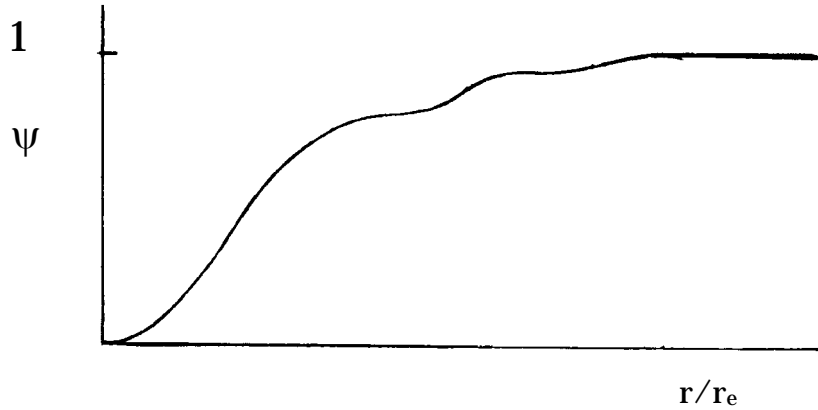


Figure 9. A composite shape function curve

In summarizing the results of the classification system and the multi-particle analysis, to this point, a conflict arises in the following way. Looking back to Eq.(3), *that relationship between the particle's rest energy and frequency appears to hold for all concentric layerons*, and it is an essential part of the so called "quantum" properties of matter. Furthermore, the tests of Stearn's, et al, discussed in Section IV, which included pionic atoms (electron replaced by a π^- bion), have been repeated, since 1957, with more massive bions. All such tests indicate that the orbit selection implied by the de Broglie frequency, discussed in Notes 3 and 4, applies in general. Thus, *all these phenomena require that any particle have one, single ℓ -wave frequency*.

On the other hand, the preceding analysis shows that if the same shape function $\psi = \varepsilon^{-r_i/r}$ used for the unons were used for each of the layers, multiple frequencies would be required, one for each layer. The resolution of this problem comes through finding a new, more general, layer ℓ -wave shape function.

The new ℓ -wave shape function for each layer takes the form,

$$\psi_i = \varepsilon^{-\frac{r_e}{r}} \left[1 + K_i E_2 \left(\frac{r}{r_e} \right) \right] , \quad (14)$$

with $E_2(r/r_e)$ representing the exponential integral of the second kind¹, r_e the effective radius of the whole multi-layer particle, and K_i an, as yet, unspecified constant. Figure 10 depicts the family of ψ_i curves with K_i as the parameter. The $K_i = 0$ curve applies to the unons, and gives the simple structure discussed earlier. However, *in multi-layer particles, each layer has a different value of K_i* ; and the radii of the layers are specified by both the particle frequency ω , which is common to all layers in any one particle, and the values of the parameter K_i , which sets the inflection radius of each potential layer. The *shapes* of the ψ_i are determined primarily by the factor $\varepsilon^{-r_e/r} = \varepsilon^{-D/\omega r}$, just as before, but *the purpose of the K_i is to allow each layer to adjust itself, relative to the total particle frequency ω , so that the layer frequencies ω_i , given by Eq.(5) match the "preferred" layer frequencies.*

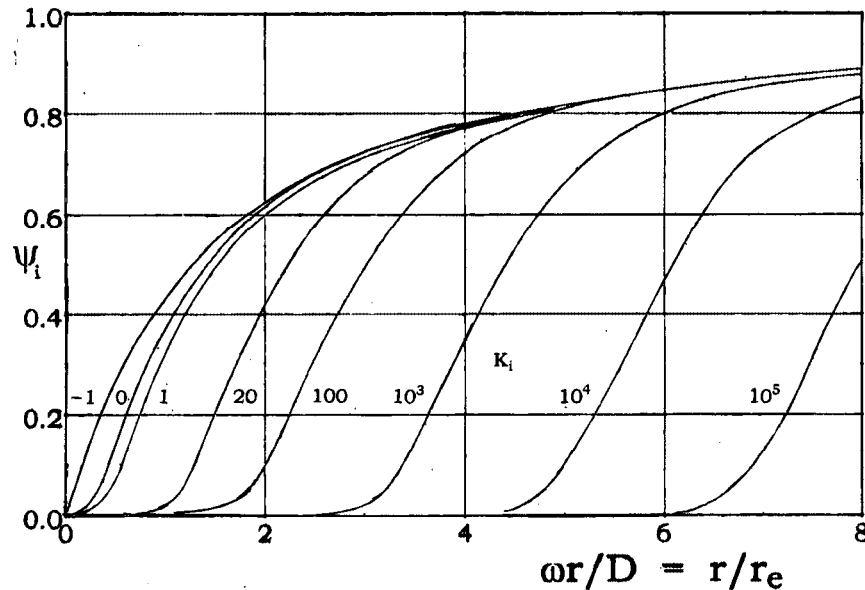


Figure 10. Layer shape function curves as a function of the parameter K_i .

1. Handbook of Mathematical Functions, National Bureau of Standards, AMS 55, p228.

Two forms of the derivative of ψ_i are required in the following,

$$\frac{d\psi_i}{dr} = \frac{r_e}{r^2} \left(1 + K_i \varepsilon^{-r/r_e} \right) \psi_i \quad , \quad (15)$$

and,

$$\frac{d\psi_i^2}{dr} = \frac{2r_e}{r^2} \left(1 + K_i \varepsilon^{-r/r_e} \right) \psi_i^2 \quad . \quad (16)$$

Determination of K_i

It was stated earlier that each potential layer can be associated with a K_i that determines the inflection radius of that layer. Starting with the gradient of the layer potential in Eq.(27), differentiating it with respect to r , setting the differential to zero and solving for K_i leads to,

$$K_i = \left(\frac{r_i}{r_e} - 1 \right) \varepsilon^{r_i/r_e} \quad , \quad (17)$$

where r_i is the inflection radius of the layer. Apparently, if K_i of that layer is a very large number, that layer is far out from the main energy of the particle. If K_i is near zero the layer is close to the effective radius r_e . For $-1 < K_i < 0$, the layer is smaller than r_e .

An even more useful way to think about Eq.(17) results from the experimentally determined fact that *each whole multi-layer particle also follows a form of Eq.(5) relating its effective radius r_e to its single frequency ω* . This is expressed as,

$$\omega r_e = D \quad . \quad (18)$$

Combining Eqs.(5), (17) and (18),

$$K_i = \left(\frac{\omega}{\omega_i} - 1 \right) \varepsilon^{\omega/\omega_i} \quad , \quad (19)$$

where the ω_i are the preferred frequencies listed in Table IV. Eq.(19) is the most convenient for determining the multi-layer particle structure.

TABLE IV

Layer	ω_i (rad/sec)	r_i (cm)
1	7.76344×10^{20}	3.52243×10^{-14}
2	1.60523×10^{23}	1.70356×10^{-16}
3	2.69981×10^{24}	1.01289×10^{-17}
4	8.508×10^{24}	3.214×10^{-18}
5	1.580×10^{25}	1.731×10^{-18}

Multi-layer Particle Charge Density

The charge density of a *concentric* multi-layer particle can be written in terms of the total particle charge q as,

$$\rho = \frac{q}{4\pi r^2} \frac{d\psi^2}{dr} \quad . \quad (20)$$

The easiest way to show this is to integrate ρ over all space to give,

$$\int_{\text{space}} \rho \, d\text{vol} = \frac{q}{4\pi} \int_0^\infty \int_0^\pi \int_0^{2\pi} \left(\frac{1}{r^2} \frac{d\psi^2}{dr} \right) r^2 \sin\theta \, dr \, d\theta \, d\alpha = q \int_0^1 d\psi^2 = q \quad . \quad (21)$$

A detailed description of the multi-layer charge density is obtained by substituting the derivative of Eq.(13) in Eq.(20), with the result,

$$\rho = \frac{q}{4\pi r^2} \left(\frac{\phi_{01}}{\phi_0} \frac{d\psi_1^2}{dr} + \frac{\phi_{02}}{\phi_0} \frac{d\psi_2^2}{dr} + \frac{\phi_{03}}{\phi_0} \frac{d\psi_3^2}{dr} + \dots \right) \quad . \quad (22)$$

Eq.(22) can be integrated over all space from $r = 0$ to $r \rightarrow \infty$, leading to,

$$q = q_1 + q_2 + q_3 + \dots \quad , \quad (23)$$

where,

$$q_i = \frac{\phi_{0i}}{\phi_0} q \quad . \quad (24)$$

From Eqs.(16) and (20) --- (22), the charge density of each layer is specified by,

$$\rho_i = \frac{q_i r_e}{2\pi} \left(1 + K_i \varepsilon \frac{-r}{r_e} \right) \frac{\psi_i^2}{r^4} \quad . \quad (25)$$

When Eq.(25) for the layer charge density is integrated over all space, the *layer charges* q_i are found to be independent of K_i , as anticipated by Eqs.(23) and (24). It is this fortunate circumstance that permits using the layer charges in the classification scheme. Thus, K_i is a parameter that can be varied after specifying the charge structure to be examined; and, although it changes the radii of the charge shells as well as the energy shells, its major effect is on the magnitudes of the layer energies.

Multi-layer Particle Potential

Some remaining details of the layer potentials not discussed earlier can be found by writing Eq.(20) in the form,

$$\rho = \frac{q}{4\pi r^2} \frac{d\psi^2}{dr} = -\nabla^2 \phi = -\frac{1}{r^2} \frac{d}{dr} \left(r^2 \frac{d\phi}{dr} \right) \quad . \quad (26)$$

This can be converted to,

$$\frac{d}{dr} \left(\frac{q}{4\pi} \psi^2 + r^2 \frac{d\phi}{dr} \right) = 0 \quad ,$$

or,

$$r^2 \frac{d\phi}{dr} + \frac{q}{4\pi} \psi^2 = \text{constant} \quad .$$

When $r = 0$, then $\frac{d\phi}{dr} = 0$ and $\psi^2 = 0$, so the constant is zero, and,

$$\frac{d\phi}{dr} = -\frac{q}{4\pi r^2} \psi^2 \quad . \quad (27)$$

Integration produces the potential distribution,

$$\phi = \phi_1 + \phi_2 + \phi_3 \dots \quad , \quad (28)$$

where,

$$\phi_i = S_i - \frac{q_i}{4\pi} \int_0^r \frac{\psi_i^2}{r^2} dr \quad ,$$

and S_i is a constant of integration. When $r = 0$, $\phi_i = \phi_{0i} = S_i$; so,

$$\phi_i = \phi_{0i} - \frac{q_i}{4\pi r_e} I_i(r) \quad , \quad (29)$$

where,

$$I_i(r) = r_e \int_0^r \frac{\psi_i^2}{r^2} dr \quad . \quad (30)$$

As $r \rightarrow \infty$, $I_i(r) \rightarrow I_i(\infty)$ and $\phi_i \rightarrow 0$. Thus,

$$\phi_{0i} = \frac{q_i}{4\pi r_e} I_i(\infty) \quad , \quad (31)$$

and,

$$\phi_i = \phi_{0i} \left(1 - \frac{I_i(r)}{I_i(\infty)} \right) \quad . \quad (32)$$

Multi-layer Particle Energy

Starting with Eq.(28), the gradient at each point in space is,

$$\nabla\phi = \nabla\phi_1 + \nabla\phi_2 + \nabla\phi_3 + \dots \quad ; \quad (33)$$

and, the total electric energy density of a *concentric* layeron is found to be,

$$\begin{aligned} \varepsilon_e = \frac{1}{2}(\nabla\phi)^2 &= \frac{1}{2}(\nabla\phi_1)^2 + \frac{1}{2}(\nabla\phi_2)^2 + \dots \\ &+ \nabla\phi_1 \cdot \nabla\phi_2 + \nabla\phi_1 \cdot \nabla\phi_3 + \dots \quad . \\ &+ \nabla\phi_2 \cdot \nabla\phi_3 + \nabla\phi_2 \cdot \nabla\phi_4 + \dots \\ &+ \dots \end{aligned} \quad (34)$$

Integrating Eq.(34) over all space gives the total energy of the particle in the form,

$$\begin{aligned}
E_0 = & E_1 + E_2 + E_3 + \dots \\
& + E_{12} + E_{13} + E_{14} + \dots \\
& + E_{23} + E_{24} + E_{25} + \dots \\
& + \dots
\end{aligned}
, \quad (35)$$

where the E_i are the layer “self” energies and the E_{ij} are the “interaction” energies, between the layers, stored in the vacuum during the particle formation process.

The energies, E_i , of the individual layers are found by using Eq.(27) to write the energy density as,

$$\varepsilon_{ei} = \frac{1}{2} (\nabla \phi_i)^2 = \frac{q_i^2}{32\pi^2} \frac{\psi_i^4}{r^4} . \quad (36)$$

Integrating Eq.(36) over all space, the *layer* self energy is found to be,

$$E_i = \frac{q_i^2}{8\pi r_e} J_i(\infty) , \quad (37)$$

where,

$$J_i(r) = r_e \int_0^r \frac{\psi_i^4}{r^2} dr . \quad (38)$$

The interaction energies, E_{ij} , can be written,

$$E_{ij} = \frac{q_i q_j}{4\pi r_e} J_{ij}(\infty) , \quad (39)$$

where,

$$J_{ij}(r) = r_e \int_0^r \frac{\psi_i^2 \psi_j^2}{r^2} dr . \quad (40)$$

In the more complicated cases, involving orbiters, in addition to the self and interaction energies, the orbiting layers are deformed and include their extra orbital kinetic energies which must be added in to give the total particle energy.

Multi-layer Particle Spin and Magnetic Moment

In Note 2, where the electron's spin was taken up, it was described as a spinning potential vortex essentially independent of the potential's distribution and the ℓ -waves. Its only pertinent characteristic was that the vortex velocity increased with r inside a very small radius ($\delta r_i \leq 0.06r_i$), and the external velocity gradually decreased as r increased ($\rightarrow 0$ as $r \rightarrow \infty$). In a multi-layer particle, the spin picture is similar for each individual layer.

The calculation for the layer spin starts with Eq.(15), Note 2, and differs from the derivation there in the substitution of Eq.(36), just above, for the energy density in terms of the new ψ_i . The layer spin can then be expressed as,

$$\sigma_i = (\kappa K_s)_i \frac{q_i^2}{12\pi c_0^2} \left[\int_0^{\delta r_i} \frac{\psi_i^4}{(\delta r_i)^3} dr + \int_{\delta r_i}^{\infty} \frac{\psi_i^4}{r^3} dr \right] , \quad (41)$$

where the first integral in the bracket is negligible with respect to the second. A very good approximation can be written in the form,

$$\sigma_i \cong (\kappa K_s)_i \frac{q_i^2}{12\pi c_0^2 r_e^2} L_i(\infty) , \quad (42)$$

where,

$$L_i(r) \cong r_e^2 \int_0^r \frac{\psi_i^4}{r^3} dr . \quad (43)$$

In the same way, the magnetic moment for each layer is found by starting with Eq.(21), Note 2, and substituting Eq.(25) for the layer charge density. The result is

$$\mu_{si} \cong (\kappa K_s)_i \frac{2}{3} \frac{q_i}{r_e c_0} M_i(\infty) , \quad (44)$$

where,

$$M_i(r) \cong r_e^2 \int_0^r \left(1 + K_i \varepsilon^{-r/r_e} \right) \frac{\psi_i^2}{r^3} dr . \quad (45)$$

As discussed in Note 2, $\kappa_i = 24\pi c_0^2 r_e / q_i = 3c_0^2 / \phi_{0i}$. This can be used with Eq.(31) to reduce Eq.(44) to,

$$\mu_{si} \cong K_{si} 8\pi c_0 \left[\frac{M_i(\infty)}{I_i(\infty)} \right] . \quad (46)$$

For any reasonable, given ω , r_e or K_i , tables of $M_i(\infty)$ and $I_i(\infty)$ reveal that the bracketed quantity has the value,

$$\left[\frac{M_i(\infty)}{I_i(\infty)} \right] = \frac{1}{2} , \quad (47)$$

to within some small error. Thus, Eq.(46) becomes,

$$\mu_{si} \cong K_{si} 4\pi c_0 . \quad (48)$$

Likewise Eq.(42) can be simplified to the reduced form,

$$\sigma_i \cong K_{si} 4\pi\phi_{0i} \left[\frac{L_i(\infty)}{I_i^2(\infty)} \right] . \quad (49)$$

Here, however, the bracketed quantity varies over a wide range; so, at first sight, Eq.(48) appears to be the natural route for establishing the value of K_{si} . In Note 2, the measured value of the electron's magnetic moment μ_s was used to establish the corresponding values of K_s and the spin σ_s . Unfortunately, *the magnetic moments of individual layers of composite particles have not been measured.*

A multi-layer particle consists of several spinning charge layers that can reorient freely and independently of each other. In the ground state of a *concentric* layeron, the magnetic moments will act to align some of the layers, tending to put them into pairs that cancel some or all of the magnetic effects. Care must be exercised, when comparing the measured magnetic moment of a whole particle to that calculated, to consider which layers are paired and which are free to reorient separately.

To avoid this difficulty, the calculation for the layer K_{si} 's is reversed from Note 2. In the Standard Model, all "quarks" have spin $1/2$,

$\sigma_i = \hbar/2 = 5.272863 \times 10^{-28}$ erg – sec , so *it is assumed here that all the layers also have spin 1/2* . Therefor, the layer *spins* are used to find the K_{si} values.

In Note 2, the electron's spin and magnetic moment were derived and related through its *gyromagnetic ratio*,

$$\frac{\mu_s}{\sigma} \cong \frac{e}{m_0 c_0} \quad . \quad (\text{electron}) \quad (50)$$

Because the individual layers in the multi-layer particles have structure similar to the electron's, by combining the above Eqs. (37), (42) and (44), the gyromagnetic ratio of each layer can be expressed in the form,

$$\frac{\mu_{si}}{\sigma_i} = \frac{q_i}{m_{0i} c_0} \left[\frac{J_i(\infty) M_i(\infty)}{L_i(\infty)} \right] \quad . \quad (51)$$

Upon checking the values of J_i , M_i and L_i for a given K_i , frequency ω or r_e , the bracketed term is found to be unity (discounting a small error) for all possible layers, with the result,

$$\frac{\mu_{si}}{\sigma_i} = \frac{q_i}{m_{0i} c_0} \quad . \quad (\text{layers}) \quad (52)$$

In terms of the values that will already be known when this stage of future calculations is reached,

$$\mu_{si} = \frac{q_i c_0}{E_i} \sigma_i \quad , \quad (53)$$

and,

$$K_{si} = \frac{\mu_{si}}{4\pi c_0} \quad . \quad (54)$$

This is the last step in the formal analysis of multi-layer particles to be presented here. There are other related quantities that can be calculated, but they do not require any further development, since they involve only well known procedures.

VIII. MULTI-LAYER PARTICLE CALCULATIONS

In the preceding analysis, five integrals that depend upon ψ_i were derived. No closed form solution for any of these is known to the writer. Instead, they are evaluated by numerical integration. The integrals are designated as, $I_i(\infty)$, $J_i(\infty)$, $J_{ij}(\infty)$, $L_i(\infty)$ and $M_i(\infty)$, and they have been used in both graphical and tabular form. The most fundamental application of the analysis starts by *choosing a particular layer/charge configuration to see what kind of particle it represents*. The analysis **predicts** its frequency ω , its rest energy E_0 , and beyond that its physical structure, charge distribution, magnetic moment etc. These are then used to determine whether or not such a particle has been observed. In every case, *the basic "existence" test is that Eqs.(3) and (35) are satisfied simultaneously*.

Evaluation of the Layer Integrals

A program that gives the values of $I_i(\infty)$, $J_i(\infty)$, $L_i(\infty)$ and $M_i(\infty)$, is presented in Note 6. By inputting a layer K_i , the program provides the integrated values. In the following the argument, ∞ , will not be indicated, and these integrals will just be designated by I_i , J_i , etc. The integrated values are not as accurate as particle physicists generally take their work, but the purpose here is to illustrate the techniques rather than to supply final particle characteristics. The program in Note 6 cannot be applied in the extreme range of K_i . Instead, certain approximations must be employed. Generally, these have a very small effect on total particle structure. For example, where the values of ω/ω_i are greater than 100, the K_i become very large, but it can be shown that

the following approximations apply,

$$I_i(\infty) \cong J_i(\infty) \rightarrow \frac{1}{\omega/\omega_i} \quad , \quad \omega/\omega_i > 100 \quad (55)$$

and, with less accuracy,

$$L_i(\infty) \rightarrow \frac{1}{2(\omega/\omega_i)^2} \quad , \quad \omega/\omega_i > 100 \quad (56)$$

and,

$$M_i(\infty) \rightarrow \frac{1}{2\omega/\omega_i} \quad . \quad \omega/\omega_i > 100 \quad (57)$$

In doing the integrals for the interaction constants J_{ij} , it is easy to show that substitution of,

$$K_{ij} = \frac{1}{2}(K_i + K_j) \quad , \quad (58)$$

allows using the J_i integral calculations for the J_{ij} , thus eliminating the need for a considerable amount of computation. In that case, an effective ω_{ij} can be defined so that,

$$K_{ij} = \left(\frac{\omega}{\omega_{ij}} - 1 \right) \varepsilon^{\omega/\omega_{ij}} \quad , \quad (59)$$

and, in the extreme ranges, it can be shown that,

$$\frac{\omega}{\omega_{ij}} \cong \frac{\omega}{\omega_i} - 0.6931 \quad , \quad \omega/\omega_i > 100 \quad (60)$$

which allows the approximation of Eq.(55) to be used for J_{ij} .

The Concentric Particle Existence Criterion

As mentioned above, the existence criterion is based upon the two energy Eqs.(3) and (35). In terms of the derived integrals, Eq.(35) becomes,

$$E_0 = \frac{1}{8\pi r_e} \left[q_1^2 J_1 + q_2^2 J_2 + \dots + 2q_1 q_2 J_{12} + 2q_1 q_2 J_{23} + \dots \right. \\ \left. + 2q_2 q_3 J_{23} + \dots \quad , \quad (61) \right. \\ \left. + 2q_3 q_4 J_{34} + \dots \right]$$

and Eq.(3) can be written as,

$$E_0 = hv = \hbar\omega \quad . \quad (62)$$

Eq.(38) indicates that the J_i values depend upon ω through ψ_i (see Figure 10), so *there are 2 independent equations for E_0 as a function of ω .*

Considerable ease in the calculations derives from a slight change of variable. By defining a quantity,

$$J = \frac{8\pi D}{e^2 \omega} E_0 = \left[\frac{q_1^2}{e^2} J_1 + \frac{q_2^2}{e^2} J_2 + \dots + 2 \frac{q_1 q_2}{e^2} J_{12} + 2 \frac{q_1 q_3}{e^2} J_{13} \dots + 2 \frac{q_2 q_3}{e^2} J_{23} + \dots \right] \quad , \quad (63)$$

Eq.(62) becomes,

$$J = \frac{4hD}{e^2} = 0.25 \quad . \quad (64)$$

For a given layer/charge configuration, Eqs.(63) and (64) can be plotted as functions of ω , as illustrated in Figure 11; and the *predicted* particle frequency ω is found at their intersection. The particle's rest energy E_0 follows from Eq.(62).

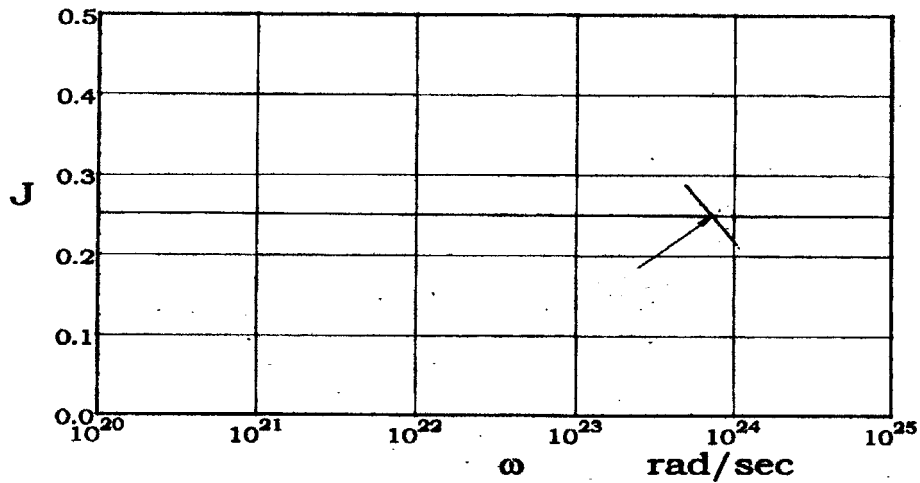


Figure 11. Eqs.(63) and (64) solved for ω

No measured data taken from a particle being investigated are used in this calculation. The only measured data involved in setting up the system are the unon frequencies and radii of TABLE II required to establish the "preferred" vacuum frequencies.

The only integrals involved in the "existence criterion" are the J_i 's and the J_{ij} 's. Table V can be used for simple calculations. More accuracy can be achieved with the program in Note 6.

TABLE V

$J_i(\infty)$

ω	J_1	J_2	J_3	J_4	J_5
4×10^{20}	0.26460	0.27145	0.27145	0.27145	0.27145
5	0.26119	↓	↓	↓	↓
6	0.25736	↓	↓	↓	↓
8	0.24891	↓	↓	↓	↓
1×10^{21}	0.23992	↓	↓	↓	↓
1.5	0.21778	↓	↓	↓	↓
2×10^{21}	0.19699	0.27145	0.27145	0.27145	0.27145
8×10^{22}	9.70431×10^{-3}	0.26501	0.27143	0.27145	0.27145
1×10^{23}	7.76343	0.26178	0.27142	↓	↓
1.5	5.17564	0.25215	0.27137	0.27144	↓
2	3.88172	0.24141	0.27134	↓	↓
3	2.58781	0.21961	0.27112	0.27142	0.27144
4	1.94086	0.19953	0.27082	0.27140	↓
5	1.55269	0.18185	0.27053	0.27139	0.2714 3
6	1.29391	0.16650	0.27011	0.27132	0.27142
8	9.70431×10^{-4}	0.14168	0.26908	0.27124	0.27139
1×10^{24}	7.76343	0.12278	0.26461	0.27108	0.27135
1.5	5.17564	0.09133	0.26358	0.27061	0.27121
2	3.88172	0.07224	0.25835	0.26995	0.27103
3	2.58781	0.05073	0.24613	0.26812	0.27048
4	1.94086	0.03892	0.23308	0.26568	0.26972
5	1.55269	0.03152	0.22019	0.26479	0.24075
6	1.29391	0.02645	0.20794	0.25941	0.26761
8	9.70431×10^{-5}	0.01999	0.18593	0.25196	0.26482
1×10^{25}	7.76344	0.01604	0.16728	0.24389	0.26152
1.5	5.17563	0.01070	0.13238	0.22325	0.25166
2×10^{25}	3.88172×10^{-5}	8.02633×10^{-3}	0.10877	0.20388	0.24071

TABLE V (Cont.)

$J_{ij}(\infty)$					
ω	J_{1j}	J_{2j}	J_{34}	J_{35}	J_{45}
4×10^{20}	0.26757	0.27145	0.27145	0.27145	0.27145
5	0.26540	↓	↓	↓	↓
6	0.26284	↓	↓	↓	↓
8	0.25673	↓	↓	↓	↓
1×10^{21}	0.24967	↓	↓	↓	↓
1.5	0.23035	↓	↓	↓	↓
2×10^{21}	0.21029	0.27145	0.27145	0.27145	0.27145
8×10^{22}	9.76974×10^{-3}	0.26782	0.27144	0.27144	0.27145
1×10^{23}	7.80543	0.26578	0.27143	↓	↓
1.5	5.19427	0.25913	0.27141	0.27141	↓
2	3.89219	0.25087	0.27137	0.27138	0.27144
3	2.59246	0.23203	0.27127	0.27128	0.27143
4	1.94347	0.21281	0.27113	0.27115	↓
5	1.55436	0.19483	0.27108	0.27097	0.27141
6	1.29507	0.17864	0.27070	0.27074	0.27137
8	9.71084×10^{-4}	0.15172	0.27103	0.27017	0.27131
1×10^{24}	7.76761	0.13092	0.26931	0.26942	0.27121
1.5	5.17749	0.09627	0.26665	0.26942	0.27091
2	3.88276	0.07555	0.26308	0.26393	0.27048
3	2.58781	0.05239	0.25399	0.25444	0.26924
4	1.94112	0.03992	0.24328	0.24380	0.26754
5	1.55286	0.03218	0.23209	0.23241	0.26663
6	1.29402	0.02692	0.22045	0.22091	0.26299
8	9.70496×10^{-5}	0.02026	0.19864	0.19897	0.25725
1×10^{25}	7.76386	0.01622	0.17922	0.17942	0.25010
1.5	5.17581	0.01214	0.14144	0.14150	0.23287
2×10^{25}	3.88182×10^{-5}	8.0712×10^{-3}	0.11544	0.11545	0.21483

Predicted Concentric Particles

It is now possible to plot the various concentric bion and trion predictions along the $J = 0.25$ line of Figure 11. First, however, the unons can be retrieved as a check on the system. As an example, choose the U_3^3 layer/charge configuration. Eq.(63) becomes $J = J_3$ and Eq.(64) is $J = 0.25$; so, from Table V, if the J_3 's for several ω 's are plotted, as in figure 11, the crossover point is found to be at $\omega = 2.70 \times 10^{24}$. The more

exact value, found from the program in Note 6, is $\omega = 2.6998 \times 10^{24}$, indicating that $U_3^{\bar{3}}$ is the τ unon. This is not surprising, since that ω was used to establish the 3rd layer preferred frequency.

Concentric Bions: The existence criterion for bion layer/charge forms is,

$$J = \frac{q_i^2}{e^2} J_i + \frac{q_j^2}{e^2} J_j + 2 \frac{q_i q_j}{e^2} J_{ij} = 0.25 \quad .$$

A typical example is the B_{23}^{12++} , which leads to,

$$J = \frac{1}{9} J_2 + \frac{4}{9} J_3 + \frac{4}{9} J_{23} \quad .$$

The graphical solution is done with a programmable hand calculator to add the three terms. Starting anywhere in Table V, an ω is chosen and the corresponding J_2 , J_3 and J_{23} terms are added. If the above sum is larger than 0.25, a larger ω is chosen. If the above sum is smaller than 0.25, a smaller ω is chosen. About 4 points, in a fairly small range of ω with 2 above and 2 below 0.25, are usually adequate. When plotted on a graph like Figure 11, the 0.25 crossover point gives the proper ω . In the case of B_{23}^{12++} , $\omega = 2.820 \times 10^{23}$. The more accurate value obtained from the program in Note 6 is $\omega = 2.8217 \times 10^{23}$.

The analysis has been used to plot the intersecting curves for all concentric bions up to, and including, the fifth layer. Figure 12 shows the result. In trying to assess which observed particles might correspond to these solutions, it must be remembered that all bions are “unstable”, i.e., they convert into lower energy particles. Later on, in calculating the proton properties, the fact that it is a truly stable particle that does not convert in its free state allows the intersection values and the observed $E_{0,\omega}$ to be essentially exact. This is not true for the concentric bions, so the results require some interpretation. For example, their mean life is about 10^{-8} to 10^{-12} seconds. If, as has been suggested earlier, they are

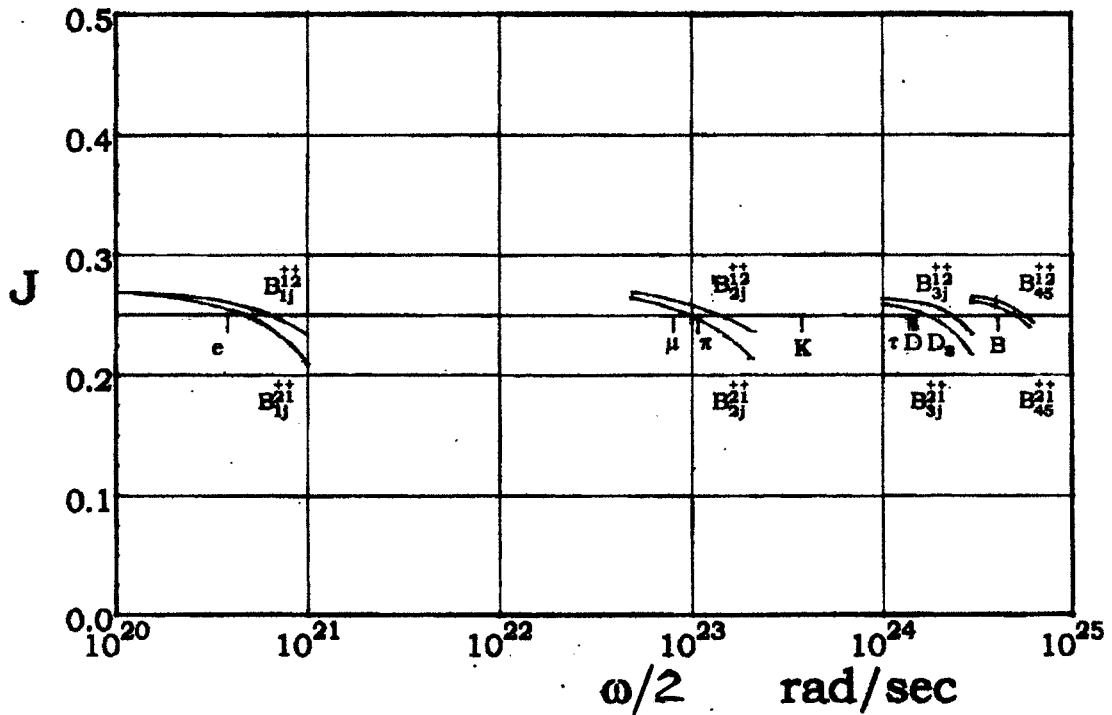


Figure 12. The Concentric Bion Solutions

basically stable, but are triggered by the datum fluctuations, the mean lives should be dependent on both the fluctuations themselves and the energy of the particles' layers. However, no solutions of the time dependent ℓ -wave equations have been carried out. Furthermore, the cutoff frequency for the datum fluctuation spectrum is not known. Thus a certain amount of guesswork is involved in the following, and *the observed particles should not be expected to exactly match the intersection points*. Notice that Figure 12 is plotted versus $\omega \setminus 2$.

Looking at Figure 12, a few significant observations can be made. For one, *a particle's outer layer establishes the major grouping pattern*. For example, B_{14}^{++} is so close in energy to B_{12}^{++} that the curves are almost identical. Likewise, B_{23}^{++} and B_{24}^{++} are essentially equal to each other. Also, Figure 12 shows that *the solutions are grouped in pairs*

distinguished only by a reversal of the charge magnitudes of the layers, i.e., B_{ij}^{2+} and B_{ij}^{1+} . Their energies are fairly closely matched, with B_{ij}^{1+} being roughly between 10% and 50% higher. Thus, *there are only eight significantly different concentric bion solutions to be observed.*

The concept involved in “conversion” is that, if B_{25}^{1+} forms, it quickly shrinks so that layer 5 becomes layer 4 or layer 3, and during this conversion its energy distortion is changing, along with its frequency, by constant interaction with the datum fluctuations, which can allow for small increases and decreases of energy. When this process is observed in an accelerator experiment, what is finally seen might be the π^+ . However, the π^+ also has a very short life, with perhaps the 12^{++} charge distortion shifting to 21^{++} and finally combining into one layer to form U_2 , the μ^+ . The μ^+ is again unstable, and so the conversion goes down the E_0/ω ladder to the positron, which is in equilibrium with the datum fluctuations.

Again, the B_{3j}^{1+}/B_{3j}^{2+} pair appear to be observed as either, D_s^+ , D^+ , or U_3 which is the τ^+ unon. The fact that the frequencies corresponding to U_4 and U_5 were estimated without being observed could explain why the predicted bions intersect so far above the related observed particles. Lower ω_i values would shift them downward.

There is an anomaly here; because, while in most cases, the conversion products are grouped fairly closely to the bion pair they originate from, the K^\pm seems too far below the $B_{3j}^{\alpha\beta}$ to be part of that group. No explanation is known for the strange location of the K^\pm on the E_0/ω ladder.

Finally, the $B_{1j}^{++} / B_{1j}^{2+}$ pair probably convert into the positron, but it is surprising that they have not been observed. Perhaps they have, but are so close to being a positron that it has been assumed that is what they are. It is clear that much more work remains in this process of identifying and classifying the various bions. Table VI lists the *concentric* bion energy ladder.

TABLE VI
CONCENTRIC BION GROUND STATES

$\omega \left(\frac{\text{rad}}{\text{sec}} \right)$	Concentric Bion	Observed Particle	E_0 (ergs)	E_0 (MeV)
1.168×10^{25}	B_{45}^{++}		1.232×10^{-2}	7,690
9.680×10^{24}	B_{45}^{2+}		1.021	6,373
8.508		(U_4^+)	8.972×10^{-3}	5,600
8.020		B^+	8.458	5,279
4.180	B_{3j}^{++}		4.514	2,817
3.200	B_{3j}^{2+}		3.375	2,107
2.870		D_s^+	3.154	1,969
2.840		D^+	2.995	1,869
2.700		τ^+	2.847	1,777
7.500×10^{23}		K^+	7.910×10^{-4}	493.7
2.820	B_{2j}^{++}		2.974	185.6
2.120		π^+	2.236	139.6
1.988	B_{2j}^{2+}		2.044	127.6
1.605		μ^+	1.693	105.7
1.370×10^{21}	B_{1j}^{++}		1.445×10^{-6}	0.901
9.360×10^{20}	B_{1j}^{2+}		9.871×10^{-7}	0.616
7.764		e^+	8.187	0.511

Concentric Trions: : The existence criterion for trion layer/charge forms is,

$$J = \frac{q_i^2}{e^2} J_i + \frac{q_j^2}{e^2} J_j + \frac{q_k^2}{e^2} J_k + 2 \frac{q_i q_j}{e^2} J_{ij} + 2 \frac{q_i q_k}{e^2} J_{ik} + 2 \frac{q_j q_k}{e^2} J_{jk} = 0.25 \quad .$$

A typical example is the T_{123}^{-++} , which leads to,

$$J = \frac{1}{9} J_1 + \frac{4}{9} J_2 + \frac{4}{9} J_3 - \frac{4}{9} J_{12} - \frac{4}{9} J_{13} + \frac{8}{9} J_{23} \quad .$$

From Table V, the J_i 's and J_{ij} 's for the range of ω from 8×10^{23} to 2×10^{24} are repeated in Table VII. The above sum is found for each ω , and plotted in Figure 13. The crossover point is at $\omega = 1.40 \times 10^{24}$ rad/s.

The more accurate value from the Note 6 program is $\omega = 1.4051 \times 10^{24}$.

TABLE VII

ω	J_1	J_2	J_3	$J_{12} \text{ \& } J_{13}$	J_{23}	J
8×10^{23}	9.704×10^{-4}	0.1417	0.2691	9.711×10^{-4}	0.1517	0.317
1×10^{24}	7.763×10^{-4}	0.1228	0.2646	7.768×10^{-4}	0.1309	0.288
1.5×10^{24}	5.176×10^{-4}	0.0913	0.2636	5.177×10^{-4}	0.0963	0.243
2×10^{24}	3.882×10^{-4}	0.0723	0.2584	3.883×10^{-4}	0.0756	0.214
Coefficient	$\frac{1}{9}$	$\frac{4}{9}$	$\frac{4}{9}$	$-\frac{4}{9}$	$\frac{8}{9}$	

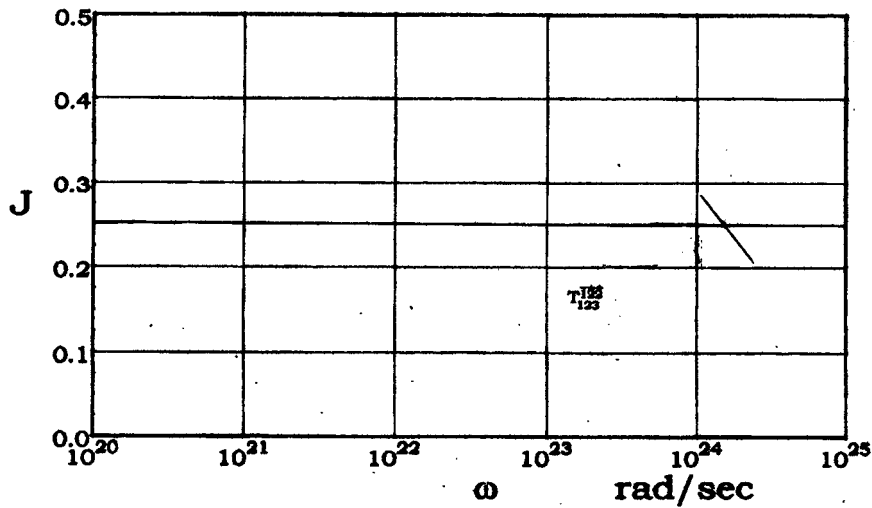


Figure 13. Predicted T_{123}^{-++} Frequency

Thus, the ω predicted for the T_{123}^{++} is just 1.43% lower than the *measured* proton frequency, $\omega = 1.42548 \times 10^{24}$, so the T_{123}^{++} may be tentatively identified as the proton.

When the existence criterion is applied to the remaining trion layer/charge forms depicted in Figure 6, the total energy of Eq.(35) is almost always too low to cross over the $J = 0.25$ level. This indicates that most other trions are orbiters requiring the added orbital kinetic energy to make up the total.

The Self-Consistent Adjustment

The close agreement between the predicted and measured proton frequencies encourages confidence in the method, and invites effort to find the source of the error. Since the system, to this point, just uses three given numbers (the e , μ and τ frequencies) to determine a fourth (the p frequency), if properly set up, it should be self-consistent and without error. One of the many possible sources of error could be the specification of the unon preferred frequencies. Of the four particles, the e and p are *stable* (the only stable particles known), and their rest energies can be measured with great accuracy. On the other hand, the μ and τ are very short-lived and their frequencies quickly shift lower during their decay, making their rest energies difficult to measure accurately. *With a small adjustment of the preferred frequencies of layers two and three the system becomes self-consistent.*

The reality is that *both might need correcting*, but a simple calculation indicates that to correct the 1.4% error, the second layer ω need only change a comparable amount, whereas the third layer ω , because of its location, must change about 40%. It is unreasonable to suppose that the measured τ energy is anywhere near that low, so only the second layer ω will be adjusted. The corrected preferred frequencies are listed in Table VIII. Future orbiter trion work might show both need changing.

TABLE VIII
SELF-CONSISTENT PREFERRED FREQUENCIES

Layer	ω_i (rad/sec)	r_i (cm)
1	7.76344×10^{20}	3.52243×10^{-14}
2	1.62973×10^{23}	1.67796×10^{-16}
3	2.69981×10^{24}	1.01289×10^{-17}
4	8.508×10^{24}	3.214×10^{-18}
5	1.580×10^{25}	1.731×10^{-18}

The corrected ω_2 is increased by 2.5%, which has only a small effect on the bion predictions expressed in Figure 12 and Table VI. For example, the ω for B_{23}^{+-} increases only 1.7%, which does not affect the relationships in Figure 12 significantly.

Self-Consistent Proton Structure

The overall analysis of proton structure can now be presented in self-consistent form. It follows a procedure somewhat different from the one used in the prediction calculation. Once the prediction shows that the layer/charge combination indicates a particular observed particle, as many characteristics of that particle are tested as possible.

The *measured* E_0 for the proton is 938.27203 MeV or 1.5032818×10^{-3} ergs. To satisfy Eq.(3), it must have a frequency $\omega = 1.4254856 \times 10^{23}$ rad/sec. If it is to be a real particle, at that frequency it must also satisfy Eq.(35) for the three layers 1,2,3, so that,

$$E_0 = E_1 + E_2 + E_3 + E_{12} + E_{13} + E_{23} \quad . \quad (65)$$

With ω_i 's from Table VIII:

$$\frac{\omega}{\omega_1} = 1.8361527 \times 10^3 \quad , \quad \frac{\omega}{\omega_2} = 8.7467592 \quad , \quad \frac{\omega}{\omega_3} = 0.52801199$$

Invoking Eq.(19):

$$\begin{aligned} K_1 &= \text{out of range} \quad , \quad K_{12} = \text{out of range} \\ K_2 &= 4.8729207 \times 10^4 \quad , \quad K_{13} = \text{out of range} \\ K_3 &= -0.80028312 \quad , \quad K_{23} = 2.4364203 \times 10^4 \end{aligned}$$

Using the program in Note 6 and the approximations in Eqs.(55) to (60):

$$\begin{aligned} J_1 &= 5.44617 \times 10^{-4} \quad , \quad J_{12} = J_{13} = 5.4482266 \times 10^{-4} \\ J_2 &= 0.09611 \quad , \quad J_{23} = 0.10153 \\ J_3 &= 0.26428 \end{aligned}$$

Eq.(18) gives $r_e = 1.9183736 \times 10^{-17}$, so the energies of Eqs.(37) and (39) are:

$$\begin{aligned} E_1 &= 3.63871 \times 10^{-7} \quad , \quad E_{12} = E_{13} = -1.45604 \times 10^{-6} \\ E_2 &= 2.56853 \times 10^{-4} \quad , \quad E_{23} = 5.42677 \times 10^{-4} \\ E_3 &= 7.06299 \times 10^{-4} \end{aligned}$$

Then, Eq.(65) leads to $E_0 = 1.50328 \times 10^{-3}$ ergs, to the accuracy limit of the program in Note 6.

Next, the program indicates that:

$$\begin{aligned} I_1 &= 5.44617 \times 10^{-4} \quad , \quad L_1 = 1.48304 \times 10^{-7} \quad , \quad M_1 = 2.72309 \times 10^{-4} \\ I_2 &= 0.11489 \quad , \quad L_2 = 5.42896 \times 10^{-3} \quad , \quad M_2 = 5.74709 \times 10^{-2} \\ I_3 &= 0.60451 \quad , \quad L_3 = 7.92868 \times 10^{-2} \quad , \quad M_3 = 0.30228 \end{aligned}$$

These are used with Eqs.(31), (53) and (54) to calculate the layer center potentials ϕ_{0i} , magnetic moments μ_{si} and spin constants K_{si} :

$$\begin{aligned} \phi_{01} &= -1.28222 \times 10^3 \quad , \quad \phi_{02} = 5.40984 \times 10^5 \quad , \quad \phi_{03} = 2.84646 \times 10^6 \\ \mu_{s1} &= 2.46567 \times 10^{-25} \quad , \quad \mu_{s2} = 6.98598 \times 10^{-23} \quad , \quad \mu_{s3} = 2.54053 \times 10^{-23} \\ K_{s1} &= 6.54492 \times 10^{-32} \quad , \quad K_{s2} = 1.85437 \times 10^{-34} \quad , \quad K_{s3} = 6.74362 \times 10^{-35} \end{aligned}$$

The next step is to try to visualize how these three layers with their spins and magnetic moments arrange themselves. The total proton spin is $1/2$ so clearly two of the layers align themselves to cancel their spins. In all likelihood, the two *inner* layers with comparable magnetic moments interact to do just that, at the same time *reducing the net magnetic field they compose*. They are the layers of greatest energy, whereas the outer layer is very much like an electron with $1/3$ the charge, and energy very much smaller than that of the two inner layers.

In measuring the proton's magnetic moment, the outer layer will precess independently at a high frequency commensurate with that usually observed for electrons. This has probably been ignored in the past. If the two inner layers were to lock together at 180° , the proton's measured magnetic moment would be the difference between μ_{s2} and μ_{s3} , or 4.44545×10^{-23} ergs/hlG, a value 11.2% lower than the observed $\mu_{sp} = 5.0056 \times 10^{-23}$ ergs/hlG. However, any misalignment results in a *larger* magnetic moment; so, if layer 3 is normally precessing in the magnetic field of layer 2, when no external field is applied, then that, coupled with a possible random disturbance from the datum fluctuations, could account for the higher measured value. The misalignment angle can be calculated from the shell structure.

Orbiters

Analysis of the orbiters, is considerably more difficult; particularly that of the *inside* orbiters, since they have *overlapping* shells on which is superimposed a dynamic orbiting motion. *The proper analysis would involve solving for the full field, transient case*. It is clear that to do this for all the possible ground state configurations and then identify the observed particles accordingly is a task that could take many man-years.

Outside Orbiters: In Note 4, it was shown that, although even there the *full field* solution of the two particle hydrogen structure is the basic

approach, it is possible to use a "separatist" approximation, i.e. a two body, planetary calculation that gives excellent results. At first glance, the *outside* bion orbiters, for example $B_{ii}^{\alpha\alpha}$, suggest the hydrogen atom and positronium as models; but it is not obvious that the same analytical approach can be used. Close proximity of the two layers adds many complications. Nevertheless, the fact that positronium lends itself to similar macroscopic analysis is encouraging, but only preliminary attempts to analyze the *outside* orbiter bions have been made. Table IX lists their *measured* properties.

TABLE IX
OUTSIDE ORBITER BIONS

Observed Particle	E_0 (ergs)	ω_l (rad/sec)	E_0 (MeV)
π^0	2.1626×10^{-4}	2.0506×10^{23}	1.3498×10^2
η	8.7711×10^{-4}	8.3172×10^{23}	5.4745×10^2
η'	1.5345×10^{-3}	1.4551×10^{24}	9.5777×10^2
η_c	4.7742×10^{-3}	4.5272×10^{24}	2.9798×10^3
Υ	1.5157×10^{-2}	1.4373×10^{25}	9.4604×10^3

Inside Orbiters: Unfortunately, the case for the inside orbiters, whose *measurements* are listed in Table X, is quite different; since the $B_{ij}^{\alpha\alpha}$ shells will surely overlap and require a full field solution. At this time, nothing more is known about the structure of these particles and it probably will be a long time before such transient solutions are available.

TABLE X
INSIDE ORBITER BIONS

Observed Particle	E_0 (ergs)	ω (rad/sec)	E_0 (MeV)
K^0 $\left\{ \begin{array}{l} K_S^0 \\ K_L^0 \end{array} \right.$	7.9736×10^{-4}	7.5610×10^{23}	4.9767×10^2
D^0	2.9873×10^{-3}	2.8328×10^{24}	1.8645×10^3
B^0	8.4582×10^{-3}	8.0204×10^{24}	5.2792×10^3
B_S^0	8.6026×10^{-3}	8.1574×10^{24}	5.3693×10^3

Trion Orbiters: Except for the clear cut case of the stable proton, the trion analysis is in an even more primitive state than that of the orbiter bions; because only a few of the trions appear to be simple, concentric layerons. Even in their ground states, most of the trions are probably orbiters. Only the briefest sketch of the trion family identification will be attempted here.

The approach taken is to *first assume that all trions are simple, concentric particles*. The calculations described previously are carried out for each one. The earlier analysis of the proton, T_{123}^{++} , is typical of the

TABLE XI
CONCENTRIC TRION FREQUENCIES

T_{ijk}^{aby}	$\bar{1}\bar{1}\bar{1}$	$\bar{2}\bar{1}\bar{1}$	$\bar{1}\bar{2}\bar{1}$	$\bar{1}\bar{1}\bar{2}$	$\bar{2}\bar{2}\bar{1}$	$\bar{2}\bar{1}\bar{2}$	$\bar{1}\bar{2}\bar{2}$	$\bar{2}\bar{2}\bar{2}$
123			n^2				p	1.47×10^{24}
124							1.47×10^{24}	1.47×10^{24}
125							1.46×10^{24}	1.48×10^{24}
134							1.88×10^{25}	1.90×10^{25}
135								
145								
234							1.67×10^{25}	2.10×10^{25}
235							2.14×10^{25}	
245								
345	4.48×10^{24}	3.38×10^{24}				3.38×10^{24}	2.20×10^{25}	8.40×10^{25}

procedure. When this is done for all the configurations represented in Figure 6, extended to include the fifth layer, *only those structures with numerical values listed in Table XI yield J values large enough to cross the 0.25 line.* This indicates that the concentric structure has energy (frequency) too low to represent a physical particle solution. On the other hand, all configurations *below* the dashed line in Table XI have energies *much greater* than any observed trion, so they are probably too compacted to do more than just explode and convert. In the $(\overset{++}{122})$ column, the proton and its two siblings are essentially the same particle, with 124 and 125 both converting almost instantaneously to the proton by shifting the inner layer out to the three position. In the $(\overset{++}{212})$ column, the 345 configuration is down 3% from Λ_c^+ and 10% from Σ_c^+ . Similarly, in the $(\overset{++}{222})$ column, the energies (frequencies) indicated are about 20% low for Δ^{++} and 60% low for Σ_c^{++} (no other particles with charge 2e have been observed). Although the $\overline{T}_{345}^{\overline{111}}$ structure has *more* energy than $\Delta^-, \Sigma^-, \Xi^-$ or Ω^- , and could appear to be any one of these with less energy during the decay process, this does not seem to be a good approach. Similar reasoning applies to the T_{345}^{211} configuration and $\Delta^0, \Lambda^0, \Sigma^0$ or Ξ^0 . Except for these last two unexplained cases, all observed trions, including those $(\overset{++}{222})$ listed, appear to be orbiters; since *the only way to bring their energies up to the observed values is to include their orbiting energies.* This has not yet been worked out for all the reasons given earlier in discussing the orbiter bions.

There are roughly 16 trions observed in the ground state (spin $\frac{1}{2}$) and 10 in the spin $\frac{3}{2}$ state that should be associated with the sixty or so low energy categories in Table XI. By far the most important of these are the proton and neutron. There is little chance of a full field, transient analysis of the neutron in the near future; but, based on a "guess" that

the so called "strong" interaction acts similarly for both protons and neutrons because each of their two outer layers have a similar form, the neutron is indicated in Table XI as being in the $(\bar{1}\bar{2}1)$ column. This is not absolutely necessary; since it might only be the *outer* layer of each trion that determines the "strong" interaction. In that case, the neutron might match a different configuration in Table XI.

One problem that arose in the quark model was the three parallel quark spins in a particle such as the Δ^{++} , which was assigned three identical u quarks, a clear violation of the Pauli exclusion principle. To resolve this problem, **the property of quark color was adopted.** *The exclusion principle is a manifestation of the single solution principle, i.e. no two identical solutions of the field equations can exist in the same place at the same time.* Referring back to Figure 1, three layers with parallel spin clearly do not represent identical solutions of the field equations, so **no need for color arises.**

IX CONCLUSION

This note hardly scratches the surface. An immense number of investigators and man hours will be needed before the picture described here can be firmed up, *so pitch in.*

ACKNOWLEDGEMENT

The author wishes to acknowledge discussions and considerable help over a period of years by:

R. L. Kirkwood	D. J. Margaziotis
L. O. Heflinger	T. Hudspeth
B. H. Mueller	R. S. Margulies
G. Ialongo	

See next page.

UNITS

To obtain the quantity in HLU, multiply the MKS quantity by the factor given. To go from HLU to MKS, divide.

	HLU	MKS
Electric Potential	$\bar{\phi}$	9.40967×10^{-4} Volts
Magnetic Vector Potential	A	2.82095×10^5
Energy	\mathcal{E}	10^7 Joules
Energy Density	ε	10 Joules
Charge	q	1.06274×10^{10} Coulombs
Charge Density	ρ	1.06274×10^4 Coulombs / m
Current	i	1.06274×10^{10} Amperes
Resistance	\mathbb{R}	8.85419×10^{-14} Ohms
Capacitance	\mathbb{C}	1.12941×10^{13} Farads
Inductance	\mathbb{L}	8.85419×10^{-14} Henrys
Electric Intensity	E	9.40967×10^{-6} Volts/m
Magnetic Induction	B	2.82095×10^3 Teslas
Electric Displacement	D	1.06274×10^6
Magnetic intensity	H	$3.54491 \times 10^{-3} \frac{\text{Amp Turns}}{\text{m}}$